Carrier spin dynamics in $CdTe/Cd_{1-x}Mn_xTe$ quantum wells

R. Akimoto, K. Ando, F. Sasaki, S. Kobayashi, and T. Tani
Electrotechnical Laboratory, 1-1-4 Umezono, Tsukuba, Ibaraki 305, Japan
(Received 27 December 1996; revised received manusript 22 May 1997)

We investigated the carrier spin dynamics in diluted magnetic semiconductor quantum wells, $CdTe/Cd_{1-x}Mn_xTe$ ($x \approx 0.35$), using femtosecond time-resolved circular dichroic spectroscopy. When the heavy-hole exciton was resonantly excited by the circularly polarized laser pulse, the positive and negative circular dichroism appeared at the heavy-hole– and the light-hole–exciton energy, respectively. They decay with different time constants, from which we succeeded in determining the spin dynamics of electrons separately from that of holes. Furthermore, we found that the electron-spin-relaxation time decreases dramatically with decreasing the well width, while the heavy-hole–spin relaxation is relatively insensitive to the variation of the well width. This strongly suggests that the electron-spin-relaxation process is governed by the s-d exchange interaction in the magnetic barrier layer, while the heavy-hole–spin relaxation by p-d exchange interaction is regulated by the degree of the mixing between the heavy- and light-hole subbands. [S0163-1829(97)05840-2]

I. INTRODUCTION

In recent years, much interest has been aimed at the physics of carrier spin dynamics in semiconductor quantum well[1–9] (QW's) and its potential application for ultrafast devices using a spin-dependent optical nonlinearity,[10,11] especially for the nonmagnetic III-V semiconductor QW's. The resent development of molecular beam epitaxy (MBE) has allowed us to obtain the high-quality II-VI diluted magnetic semiconductor (DMS) QW's, in which it is possible to control an interacting region between the carrier spin and the magnetic ion spin embedded in the structures, and various spin-dependent optical properties such as the giant Zeeman effect and the magnetic polaron effect and have been observed in the structure-controlled manner. The photoinduced magnetization experiments,[12,13] in which the injection of the spin-polarized carriers induces the magnetization of the magnetic ions, has confirmed the existence of the spin-flip process between the carrier spin and the embedded magnetic ions. In connection with those experiments, the carrier spin-relaxation process is expected to be modified strongly by the magnetic ion through the spin-flip process.

In a QW, the degeneracy between a heavy-hole (hh) and a light-hole (lh) exciton is lifted owing to the different quantum confinement between the hh and lh and the biaxial strain effect. Accordingly, electrons and holes can be created with a full spin polarization in the conduction and the valence band, respectively, by the circularly polarized light. In the previous studies of the relaxation of spin polarization (or spin relaxation) in the QW's, the time-resolved absorption change using the circularly polarized pump and probe pulse has been employed, where the wavelengths of the pump and probe pulse are the same and are resonant with the hh exciton.[1–4] In addition, the time-resolved luminescence measurement has been employed, where the hh exciton is excited resonantly by the circularly polarized pulse and then the decay of the circular polarization of the luminescence is measured.[5–9] In the two measurements for the case of the undoped QW's, both the electron and hh spin contribute, simultaneously, to the spin-relaxation at the hh-exciton energy. A possible way to isolate the electron-spin relaxation from the hh spin relaxation in $GaAs/Al_xGa_{1-x}As$ QW's, is to use p-doped QW's for the electron-spin relaxation and n-doped QW's for the hh spin relaxation.[9] However, the spin-relaxation mechanism in the doped QW's should be quite different from that in undoped QW's due to carrier-impurity scattering, the Coulomb screening of the carriers, and so on. Actually, the hh spin relaxation was measured directly in undoped $Al_xGa_{1-x}As/AlAs$ QW's having type-II structure by using the fast intervalley scattering of electron from the Γ point of the well layer to the X point of the barrier layer.[3] This is, however, the specific case applicable only for the $Al_xGa_{1-x}As/AlAs$ QW's and is not the general case. We present a different approach to measure the electron-spin relaxation separately from the hh-spin relaxation by using the femtosecond time-resolved circularly dichroic (CD) spectra. It has been shown that the time-resolved CD enables to separate completely the effect of screening and phase-space filling.[14] So, we can examine the population difference between the degenerate electron- and hh-spin state, and their time evolution in time resolved CD spectra.

Furthermore, we present the experimental results of the carrier spin relaxation which is affected by the magnetic Mn spin through the s-d or p-d exchange interaction. The interaction is characteristic of DMS's such as $Cd_{1-x}Mn_xTe$.[15] Theoretical prediction has shown that the electron Mn spin (s-d) exchange interaction is a very efficient spin-flip scatter for electrons, although the hole-spin scattering caused by the hole Mn spin (p-d) exchange interaction becomes inhibited in a strong confinement limit.[17,18] In the $CdTe/Cd_{1-x}Mn_xTe$ multiple QW structure studied here, the wave functions of an electron and a hole in a well layer penetrate into a barrier layer and their spins interact with the Mn spins embedded in the barrier layer through the s-d or p-d exchange interaction. So we can control the degree of the carrier penetration depth by changing the QW width and observe the change of the spin-relaxation behavior. The experimental data for the electron-spin relaxation are clearly accounted for in consid-

eration of the penetration of the electron wave function into the magnetic barrier layer and the subsequent s-d exchange interaction. On the other hand, the hole-spin relaxation is explained taking the hh and lh subband mixing and the p-d exchange interaction into account.

II. EXPERIMENTAL DETAILS

A. Samples

The (100)-oriented $CdTe/Cd_{1-x}Mn_xTe$ ($x \approx 0.35$) multiple QW's are grown by a MBE method on a GaAs(100) substrate with $\sim$2000-Å-thick CdTe and $\sim$2000-Å-thick $Cd_{1-x}Mn_xTe$ buffer layers and capped with an $\sim$2000-Å-thick $Cd_{1-x}Mn_xTe$ layer. A series of samples consists of 20 periods of alternating an CdTe well layers and a 45-Å-thick $Cd_{1-x}Mn_xTe$ barrier layers. The width of the CdTe well (L_z) is varied from 40 Å to 123 Å in order to sufficiently control the number of the manganese ions interacting with the carrier spin through the carrier penetration degree into the barrier layer. For instance, the Zeeman splitting of the hh exciton absorption band in the sample with a well width of 40 Å amounts to 11.3 meV, while it amounts to 0.64 meV for the sample of 123 Å at 5 K and 5 T. This result shows that changing the well width is enough to investigate the effect of the carrier spin relaxation concerning the s-d or p-d exchange interaction. The substrate is selectively etched away to perform the pump-probe absorption measurements with a transmission configuration.

B. Time-resolved pump-probe experiments

We use two different types of femtosecond time-resolved pump-probe experiments. One is the pump-probe experiment, in which the probe pulse has a continuum spectrum to measure a transient CD spectrum. From this we can examine selectively the population differences between the degenerate spin states of an electron and a hh, and their time evolution. The other is the degenerate pump-probe experiment, in which the wavelength of the probe pulse is the same as that of the pump pulse. The degenerate pump-probe experiment is employed to obtain a better signal-to-noise ratio in the measurement of the carrier spin dynamics at the hh exciton energy.

1. Pump-probe experiment for the measurement of the time-resolved CD spectrum

The pump-probe experiments are performed using a laser system of an optical parametric generator and amplifier (OPG/OPA) excited by a Ti:sapphire regenerative amplifier with a repetition rate of 1 kHz. The output pulse from the OPG/OPA with 0.15 mJ/pulse is passed through a β-barium-borate crystal and the resultant second-harmonic and remaining fundamental beams are split by a dichroic mirror. The second-harmonic beam is used as a pump pulse, while the fundamental beam is focused into the sapphire plate in order to generate a probe pulse having a continuum spectrum. To obtain a circularly polarized continuum probe pulse, the linearly polarized probe pulse is passed through a quarter-wave Fresnel rhomb. The polarization of the pump pulse is fixed to right circularly polarization (σ^+), while that of the probe pulse is switched either to left (σ^-) or right (σ^+) circularly polarization. The pump and probe pulses are focused onto samples about 400 μm and 100 μm in diameter, respectively, which are held at 6 K in a cryostat. The probe beam passing through the sample is dispersed by a 0.25-m spectrometer equipped with a charge coupled device camera to obtain differential transmission spectra. The cross correlation between the pump and probe pulse is about 200 fs, which gives the time resolution. The spectral width of the pump pulse is about 20 nm and its wavelength of the pump pulse is tuned to the lower-energy side of the hh-exciton absorption line in order to excite only the hh exciton resonantly [see Fig. 2(b)]. Thus there is no excitation of the lh excitons. The excitation density of the pump pulse is about 4 $\mu J/cm^2$.

2. Degenerate pump-probe experiment

The time-resolved and the spin-dependent absorption measurements are performed using a mode-locked Ti:sapphire laser with the repetition rate of 76 MHz. The duration of the laser pulse is 130–200 fs depending on the wavelength, which is tuned to the lower-energy side of the hh-exciton absorption band. The repetition rate of the laser pulse train is reduced to 3.17 MHz using a pulse picker in order to reduce the heating of the sample (especially the temperature of Mn spin system[19]) and to obtain stronger signals of pump-induced absorption saturation. The pulse-picked train is divided into the pump and probe beams. The energy of the pump pulse is about 0.7 $\mu J/cm^2$ in front of the sample. The pulse energy of the probe beam is reduced to one-tenth of the pulse energy of the pump pulse. The circular polarization of the probe pulse (σ^+) is fixed, while that of the pump pulse is changed to σ^+ or σ^-. The pump and probe pulses are focused onto a sample about 120–130 μm in diameter. The pump beam is chopped at 1.5 kHz and the signal due to the pump-induced change in the transmitted probe intensity is obtained using phase-sensitive detection. The sample is held at 5 K in the cryostat.

III. SELECTION RULES FOR THE OPTICAL TRANSITIONS AND CARRIER SPIN RELAXATION

The electronic energy levels of the conduction- and valence-band edges at the Γ point in the $CdTe/Cd_{1-x}Mn_xTe$ QW structure is shown in Fig. 1. Because of the selection rules for the optical transitions, the circularly polarized light couples the distinct angular momentum states between the conduction and valence bands. When the strong σ^+ pump pulse resonantly excites the hh-exciton level, the $-1/2$ electron state and the $-3/2$ hh state are instantaneously created. Due to the occupation of these states and their phase-space filling effect,[16] the absorption of the σ^+ probe pulse saturates at the hh-exciton energy. Subsequently, the electron spin relaxes from the 1/2 state to the $+1/2$ state and the hh spin relaxes from the $-3/2$ state to the $+3/2$ state. As a result, the saturation of the σ^+ probe pulse starts to decrease and simultaneously the absorption of the σ probe pulse starts to saturate at the hh exciton energy owing to the occupation in these state by both the electron- and the hh-spin relaxation. The difference of the absorption saturation between the σ^+ and σ^- probe pulse and their time dependence makes the transient CD spectrum. At the same time, the absorption of the σ^- probe pulse at the lh exciton energy is also saturated

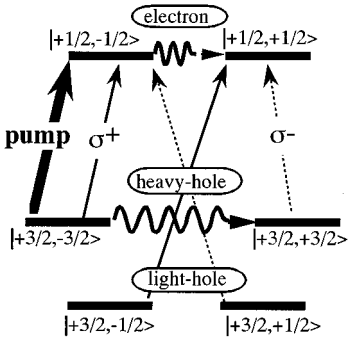

FIG. 1. Angular momentum states $|J,J_z\rangle$ of the conduction and valence bands at the Γ point in a $CdTe/Cd_{1-x}Mn_xTe$ quantum well. The selection rule for the optical transition is shown. The initial dynamical process of the carrier spin relaxation is also shown, after the resonant excitation of the heavy-hole exciton by the σ^+ circularly polarized pump pulse.

instantaneously with the same resonant condition. Only the $-1/2$ electron state contributes to this saturation because lh excitons are not excited and hence there is no occupation of the lh state. Since the electron spin relaxes from the $-1/2$ state to the $+1/2$ state, the absorption of the σ^+ probe pulse saturates owing to the occupation of the $+1/2$ electron state. Therefore, we can measure directly the electron-spin relaxation by observing the time dependence of the CD spectrum at the lh-exciton energy, while we measure the convolution of the electron-spin and hh spin relaxation by observing the time evolution of the CD at the hh exciton energy. Furthermore, we can deduce even the hole spin relaxation by comparing the time evolution of the CD spectrum observed at the lh-exciton energy with that observed at the hh-exciton energy.

IV. RESULTS AND DISCUSSION

A. Separation of electron-spin and hh-spin dynamics

Several differential transmission spectra (DTS) for different pump-probe delay times are shown in Fig. 2(a). The solid curves are the DTS where the hh exciton is pumped resonantly by the σ^+-polarized pulse and DTS are measured by the σ^+-polarized probe pulse, namely, $(\sigma^+_{\text{pump}},\sigma^+_{\text{probe}})$, while the dashed curves are the DTS in the case of (σ^+,σ^-). The linear absorption and pump spectra are also shown in Fig. 2(b). The DTS signal oberved at 1.655 eV and 1.695 eV in Fig. 2(a) correspond to the hh exciton and the lh-exciton energies, respectively. The DTS within 4 ps after the excitation show the different spectral response depending on the circular polarization of probe pulse around the hh- and lh-exciton energy and this spectral difference makes the transient CD spectrum. Further, the transient CD spectrum disappears at 12 ps. This means that the carrier spin relaxation is completed during this time scale.

The peak intensity of the DTS at the hh exciton is much larger than that at the lh exciton. It can be partly attributed to the difference in the oscillator strength between the hh and the lh exciton. Moreover, the effect of the phase-space filling for the electron and the hh state also accounts for the result. The origin of the differential transmission (DT) at the hh-

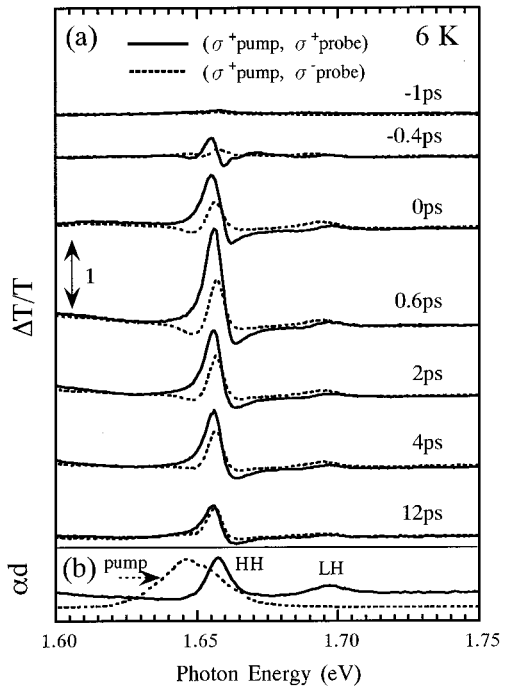

FIG. 2. (a) Differential transmission spectra (DTS) for several pump-probe delay times at 6 K. The pump pulse is σ^+ circularly polarized. The solid line and the dashed lines show the DTS for the σ^+ and σ circularly polarized probes, respectively. (b) The linear absorption spectrum (solid line) and the pump laser spectrum (dashed line) are also shown.

exciton energy is due to the occupation of both the electron and the hh states, while the DT at the lh-exciton energy is due to the occupation of only the electron state. The effect of the phase-space filling determines the DT intensity. Therefore, if the effect of the phase-space filling for the hh state is much stronger than that for the electron state, it makes the different DT intensity between the hh- and the lh-exciton energies.

Figures 3(a) and 3(b) show the time evolution of the DT at the hh- and the lh-exciton energies, respectively, for (σ^+,σ^+) and (σ^+,σ^-). It should be emphasized that the DT intensity for (σ^+,σ^+) is larger than that for (σ^+,σ^-) at the hh-exciton energy [Fig. 3(a)], whereas the DT intensity for (σ^+,σ^+) is smaller than that for (σ^+,σ^-) at the lh-exciton energy [Fig. 3(b)] in the early times after the excitation. These experimental results clearly indicate that the initial populations of the $-1/2$ electron state and the $-3/2$ hh state are larger than those of the $+1/2$ electron state and the $+3/2$ hh state, respectively. It is consistent with the selection rules of the optical transition and the spin relaxation as shown in Fig. 1; we actually observe the difference of the population and its time evolution between these spin states.

The DT intensities for (σ^+,σ^-) at the hh-exciton energy and for (σ^+,σ^+) at the lh-exciton energy, which are shown by the open circles in Fig. 4(a) and the closed circles in Fig. 4(b), respectively, also rise within the pump pulse-duration. However, this does *not* mean that the $+1/2$ electron state and the $+3/2$ hh state are also almost instantaneously populated within the pumping time, although we assume that the pump pulse produces only the population at the $-1/2$ electron state and the $-3/2$ hh state. The line-shape analysis on the hh-

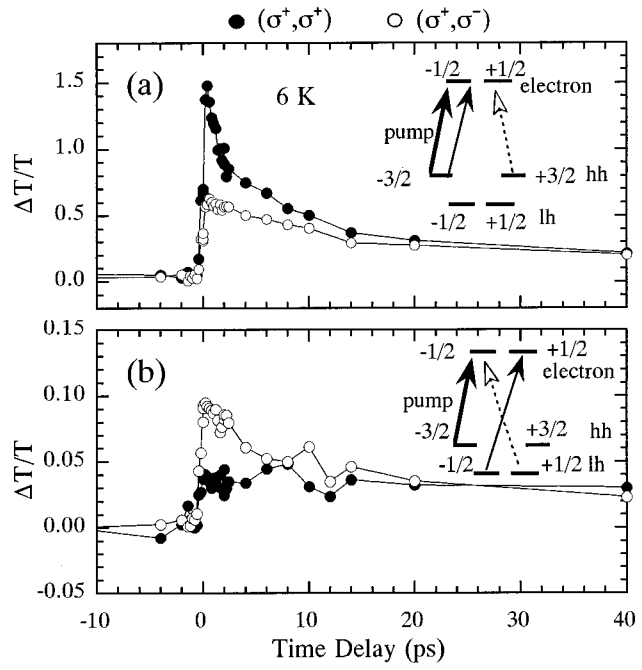

FIG. 3. Time evolution of the differential transmission (DT) at (a) the heavy-hole–exciton energy and the (b) light-hole–exciton energy. The closed and the open circles denote the DT for the σ^+ and σ^- circularly polarized probes, respectively, when the heavy-hole exciton is excited by the σ^+ polarized pump pulse. The energy diagrams show the relation between the pump and probe pulse regarding their energy and circular polarization.

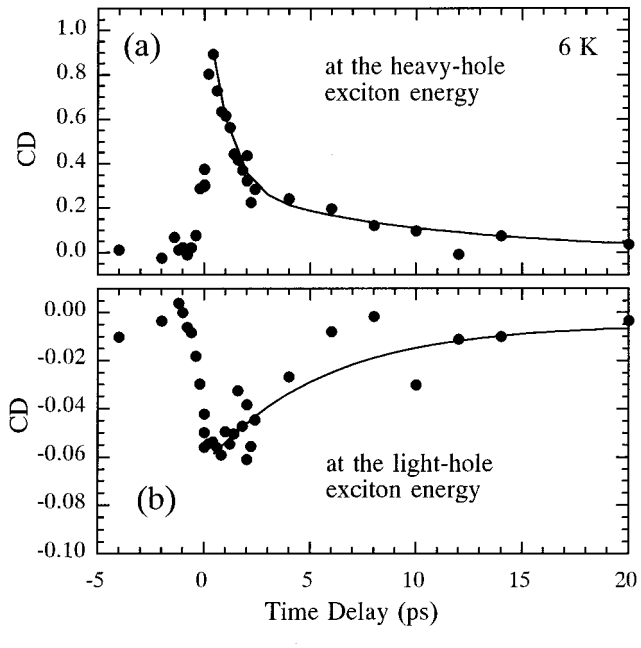

FIG. 4. Time evolution of the circular dichroism (CD) at (a) the heavy-hole–exciton energy and (b) the light-hole–exciton energy. The CD is obtained by the subtraction of the differential transmission for (σ^+,σ^+) from that for (σ^+,σ^-) of the data in Fig. 3. The curves in the figure are the results of the fitting.

exciton absorption band shows that CD spectrum comes from the fact that the blueshift, the decrease of the oscillator strength, and the broadening occur spin dependently. Furthermore, the unexpected initial rise of the DT intensity for (σ^+,σ^-) is due not to the peak shift but to the decrease of the oscillator strength and the broadening. The blueshift for (σ^+,σ^-) increases gradually from zero and coincides with the blueshift for (σ^+,σ^+) after a time delay longer than 10–20 ps, while the blueshift for (σ^+,σ^+) occurs suddenly after the excitation, which is clearly seen on the dispersive line shape of DTS in Fig. 2(a). These peak shifts are directly confirmed by the peak position of the time-resolved absorption band for the hh exciton. These blueshifts suggest that the σ^+ pump pulse produces only the population at the $-1/2$ electron state and the $-3/2$ hh state just after the excitation and the blueshifts in the time-resolved absorption band appear to reflect the population dynamics more directly than the decrease of the oscillator strength and the broadening. The physical origin of the blueshift is known as a repulsive part of many-body effect having its origin in the Pauli exclusion principle acting on the Fermi particles (electron and hh) forming the hh exciton.[16] The attractive part of the many-body effect (van der Waals interaction) can be considered to be approximately zero since the time-resolved absorption band for (σ^+,σ^-) shows no redshift but a blueshift from zero gradually after the excitation. This is consistent with the theory concerning the renormalization of exciton energy due to the many-body effect in an ideal two-dimensional system.[16] The broadening comes from a collision between electrons or holes constituting excitons that are participating in the collision. In our analysis, it is also found that the broadening of hh-exciton band is more efficient for (σ^+,σ^-) than that for (σ^+,σ^+). This means that the efficiency of the collision between two particles having opposite spin states is larger than that for two particles having parallel spin states. This conclusion is consistent with the result presented by Kawazoe *et al.*, in which they insist that up-spin holes selectively collide with down-spin holes in $Al_xGa_{1-x}As$/AlAs QW's having type-II structure.[3]

Figures 4(a) and 4(b) show the time evolution of the CD spectrum at the hh- and lh exciton energy, respectively. The sign of the CD spectrum is positive at the hh-exciton energy, while it is negative at the lh exciton energy. Although a DT originates from the effect of both screening (spin independent) and phase-space filling (spin dependent), a CD spectrum comes from only the phase-space filling.[16] It should be pointed out that the CD at the hh-exciton energy [Fig. 4(a)] reflects the time evolution of both the population difference between the electron-spin states and the difference between the hh-spin states. Therefore, at the hh-exciton energy, we fit the shape of the decay with the double exponential curves and their time constants are deduced to be 0.92 ± 0.23 ps and 10.0 ± 4.3 ps. To determine which time constant the electron- and hh-spin relaxation contribute to, it is useful to observe a CD decay at the lh-exciton energy since the CD decay at the lh-exciton energy reflects only electron-spin dynamics. In fact, there is no steep decrease of the CD signal at the lh-exciton energy, while it is observed at the hh-exciton energy. So we attribute the fast decay component at the hh-exciton energy to the hh-spin relaxation and consequently the slow

TABLE I. Comparison of the electron-spin and the heavy-hole (hh)–spin-relaxation time in $CdTe/Cd_{1-x}Mn_xTe$ quantum wells (QW's) with those in $GaAs/Al_{1-x}Ga_xAs$ QW's, superlattices (SL's), and other II-VI nonmagnetic QW's. The determination of the electron-spin and hh–spin-relaxation time in undoped $GaAs/Al_{1-x}Ga_xAs$ QW's and SL's is based on the assumption that the hh-spin relaxation should be much faster than the electron-spin-relaxation time due to the strong spin-orbit coupling and the band mixing at the valence band.

Sample	Well/Barrier (Å)	Electron (ps)	hh (ps)	Temperature (K)
p-doped $GaAs/Al_{0.3}Ga_{0.7}As$ QW's[a]	60/280	150		10
n-doped $GaAs/Al_{0.3}Ga_{0.7}As$ QW's[a]	50/280		4	10
undoped $GaAs/Al_{0.3}Ga_{0.7}As$ QW's[b]	80/210	150	1	4.5
undoped $GaAs/Al_{0.3}Ga_{0.7}As$ QW's[c]	80/300	120	50	4.2
undoped $GaAs/Al_{0.3}Ga_{0.7}As$ SL's[c]	30/30	250	35	4.2
undoped $Zn_{0.77}Cd_{0.23}Se/ZnSe$ single QW's[d]	120/	27	4.6	4.6
undoped $CdTe/Cd_{0.65}Mn_{0.35}Te$ QW's[e]	66/45	10	0.92	6

[a]Reference 9.
[b]Reference 8.
[c]Reference 2.
[d]Reference 24.
[e]Present study.

decay component to the electron-spin relaxation. Furthermore, to check whether the assignment is appropriate, we fit the CD decay at the lh-exciton energy with a single exponential curve and the time constant is determined to be 5.6 ± 2.6 ps. Since this time constant coincides with the slow decay time constant observed at the hh-exciton energy within the experimental accuracy, we can reconfirm that the above assignment is appropriate and the slow decay component at the hh-exciton energy comes from the electron-spin relaxation.

Table I shows the comparison of the electron- and hh-spin-relaxation times in $CdTe/Cd_{1-x}Mn_xTe$ QW's with those in $GaAs/Al_{1-x}Ga_xAs$ QW's, superlattices and other II-VI nonmagnetic QW's reported previously. In any case the in GaAs system, the relaxation time of hh-spin is much faster than that of the electron spin. This rapid hh-spin scattering is assumed to be due to very strong spin-orbit effect and the band mixing in the valence band. Note that the determination of the electron- spin and hh-spin-relaxation time in the undoped GaAs system is based on this assumption. In $CdTe/Cd_{1-x}Mn_xTe$ QW's, the situation is similar to that in the GaAs system in that the hh-spin relaxation is much faster than the electron-spin relaxation. However, the absolute value in the electron-spin-relaxation time in $CdTe/Cd_{1-x}Mn_xTe$ QW's is at least ten times and about three times faster than that in GaAs system and $Zn_{1-x}Cd_xSe/ZnSe$ QW, respectively, at low temperature. So the additional relaxation mechanisms contribute to the electron-spin scattering in $CdTe/Cd_{1-x}Mn_xTe$ QW's. The electron Mn spin scattering is one plausible mechanism. In the process of the spin scattering, the electron-spin scattering occurs in the barrier layer as the consequence of the penetration of the electron wave function into the magnetic barrier layer. In the next sub-section we investigate the effect of the carrier penetration into the magnetic barrier layer for a series of samples having various well widths in order to elucidate the carrier spin relaxation due to the carrier Mn spin interaction. For this purpose, we employ the degenerate pump probe method resonant with the hh-exciton energy to obtain the CD signal with a better signal-to-noise ratio.

B. Well width and temperature dependence of the carrier spin relaxation

Figure 5 shows the time evolution of the CD spectrum at the hh-exciton energy for all the samples at the present study. The time evolution of the CD spectrum is measured by the degenerate pump-probe experiment at 5 K. The decay profile can be characterized by the fast and the slow components.

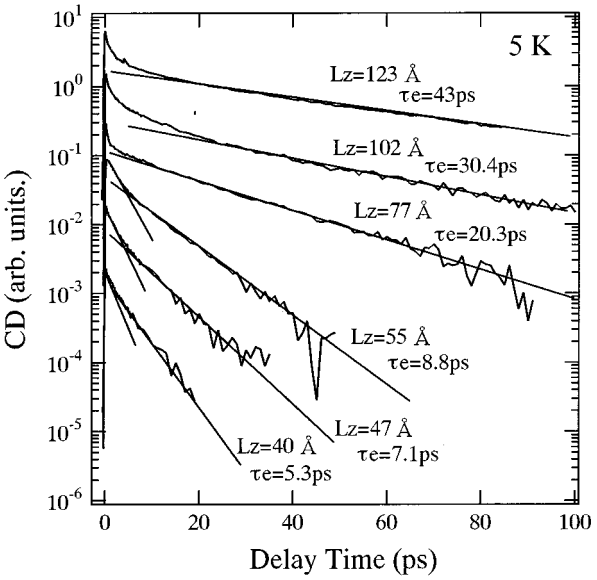

FIG. 5. Time evolution of the circular dichroism (CD) at the heavy-hole–exciton energy for samples with various well widths (L_z) at 5 K. The CD is measured by the degenerate pump-probe experiment. The notation τ_e is the time constant for the electron-spin relaxation. The rapid initial decay superimposed on the electron-spin relaxation is due to the heavy-hole spin relaxation.

For instance, the time constants of 2.0 ps and 8.8 ps are obtained from the fitting for the sample with the well width of 55 Å. We identify the fast decay constant with the hh-spin-relaxation time and the slow decay constant with the electron-spin-relaxation time, as shown in the preceding subsection by means of the time-resolved CD spectra and as in the case of the identification for the $GaAs/Al_{1-x}Ga_xAs$ Qw's.[1,2,9,20] Decreasing the well width from 123 Å to 40 Å, a dramatic decrease of the electron-spin-relaxation time from 43 ps to 5.3 ps is clearly observed. The rapid initial decay superimposed on the electron-spin relaxation is due to the hh-spin relaxation. In contrast with the behavior of the electron-spin relaxation, the hh-spin relaxation time of $\sim 2\,ps$ is almost unchanged with an increase of the well width from 40 Å to 55 Å. Increasing the well width further, the hh-spin relaxation shows nonexponential decay for the samples with $L_z = 102$ and 123 Å. This hh-spin-relaxation behavior will be discussed later.

We discuss two possible origins of our finding that the electron-spin-relaxation time is shortened by decreasing the well width. One is the s-d exchange interaction, which is characteristic for DMS QW's. The other is the D'yakonov-Perel (DP) mechanism, by which it is possible to account for the decrease of the electron-spin-relaxation time with decreasing well width in $GaAs/Al_{1-x}Ga_xAs$ QW's.[21] At first, we rule out the latter mechanism for the following reasons. The DP mechanism predicts that the decay rate is proportional to $E_1^2\tau$, where the E_1 is the first confined electron energy in the, QW and τ is the electron momentum relaxation time. Our results show that the decay rate is approximately proportional to $E_1^{1.23}$ rather than E_1^2, where E_1 is calculated by a simple Kronig-Penney model including the biaxial stress effect in the grown layer.[22,23] Further, the DP mechanism is thought to become efficient for the sample with the high electron mobility, but this is not the present case. These reasons rule out the DP mechanism in the present results.

Figure 6 shows the well width dependence of the decay rate of the electron-spin relaxation together with the electron probability density integrated over the barrier. The electron probability density is calculated by the same model discussed above. As seen in Fig. 4, the decay rate of the electron-spin relaxation is scaled linearly with the electron probability density integrated over the barrier. This strongly suggests that the electron-spin relaxation is caused by the electron penetration into the barrier and the subsequent interaction with the origin that lies in the barrier: the s-d exchange interaction between the electron spin and Mn spin. The s-d exchange interaction has terms such as $s_+S_- + s_-S_+$ of the s-d exchange Hamiltonian, which enables the electron spin to flip from $s_z = -1/2(+1/2)$ to $s_z = +1/2(-1/2)$ and Mn spin to flip from S_z to $S_z - 1(S_z + 1)$, simultaneously, where s_z and S_z are the third components of the electron and Mn spins, respectively. So the electron-spin relaxation due to the s-d exchange interaction is possible. The theory concerning the spin relaxation of the conduction electron in $CdTe/Cd_{1-x}Mn_xTe$ already has been given.[17] It predicts that the electron-spin-relaxation rate is approximately proportional to the square of the electron probability density integrated over the magnetic barrier layer and the calculated relaxation time is much larger than 1 ns

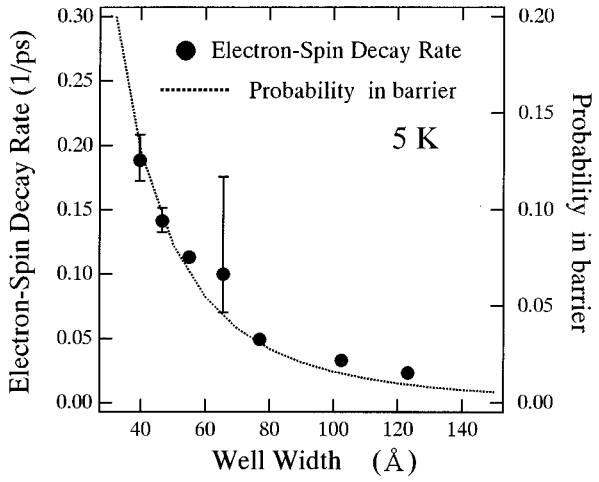

FIG. 6. Well width dependence of the electron-spin-relaxation rate and its probability density integrated over the barrier. The electron-spin-relaxation rate at $L_z = 66$ Å is taken from the result in Fig. 4.

for the sample with $L_z > 50$ Å. It is obvious that the theory cannot explain the well width dependence of the experimental results. The reasons for this discrepancy between the theory and the present results is partly attributed to the coupling of the electron wave functions between neighboring wells since the present QW's have the 45-Å-thick barrier layer not enough to prevent the coupling. So a bulklike description for the electron Mn spin-flip relaxation should be included for the theory. Regardless of the discrepancy, the present results reveal clearly the direct correlation between the spin relaxation rate of the electron and its penetration degree into the magnetic barrier layer, which suggests that Mn spins should be the spin-flip scatter for the electron. Furthermore a similar trend is observed in $Zn_{0.77}Cd_{0.23}Se/ZnSe$ single QW's with insertion of the MnSe layer, although the exact correlation between the carrier spin relaxation time and its overlap on Mn ion is not shown.[24] This result supports our interpretation that the electron spin-relaxation is shortened by the interaction between carriers and Mn ions.

We turn our attention to the hh-spin relaxation behavior as shown in Fig. 5. There is no decrease of the hh-spin-relaxation time with decreasing well width. Although the hh probability density integrated over the barrier is increased with decreasing well width, the p-d exchange interaction does not seem to affect the hh-spin relaxation compared to the electron-spin relaxation. This is qualitatively reasonable, taking the following reason into account. The hh-spin relaxation from $-3/2(+3/2)$ to $+3/2(3/2)$ via the p-d exchange interaction is forbidden since the p-d exchange interaction couples spin states between $\Delta J_z = 1$ or -1. However, the hh-spin relaxation via the p-d exchange interaction becomes possible when the hh wave vector is apart from zero through the mixing between the hh and lh subbands.[2] The degree of the mixing of the hh and lh subbands increases with decreasing the splitting between the hh and lh subbands (i.e., increasing the well width). Consequently, the hh-spin-relaxation rate has the trade-off relation between the hh

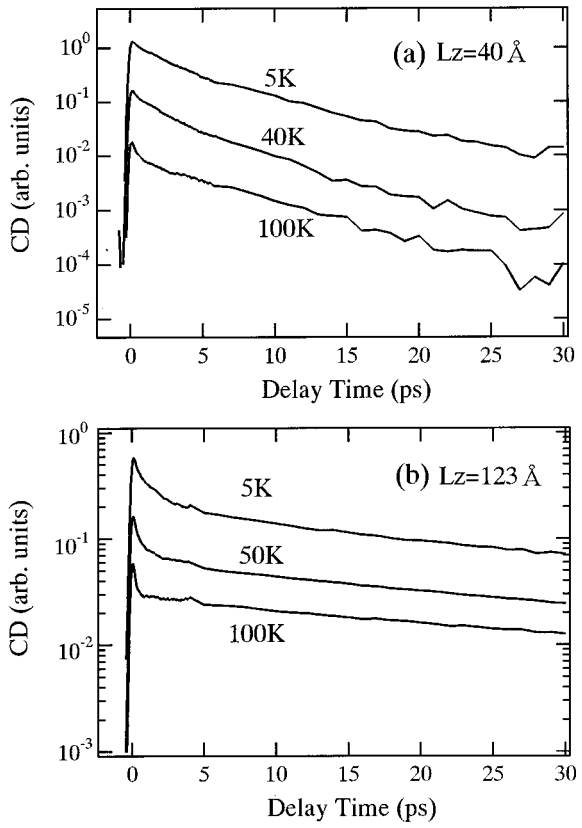

FIG. 7. Temperature dependence of the circular dichroism (CD) at the heavy-hole–exciton energy for the sample with (a) $L_z = 40$ Å and (b) 123 Å. The CD is measured by the degenerate pump-probe experiment.

penetration degree into the barrier (i.e., interaction strength of the p-d exchange) and the hh-lh splitting (i.e., degree of mixing between hh and lh subbands) when the well width is changed. This is the reason presumably why the hh-spin relaxation is insensitive to the well width. Furthermore, we performs the spin-relaxation measurements at the exciton transition energy, so this actually means that the hh states whose wave vector spreads up to $\sim 1/a_0$, with a_0 the exciton Bohr radius, are probed. As mentioned above, the hh-spin-relaxation rate depends considerably on the degree of the mixing between the hh and lh subbands and consequently on the hh wave vector. So the nonexponential decay behavior is observed for the samples for the wider wells of $L_z = 102$ and 123 Å. In these samples, the range of the hh wave vector, in which the mixing between the hh and lh subbands cannot be ignored, is thought to be compared with $\sim 1/a_0$.

Figure 7 shows the temperature dependence on the time evolution of the CD spectrum for the sample with $L_z = 40$ Å [Fig. 7(a)] and 123 Å [Fig. 7(b)], having the narrowest and widest confined well width in the present study, respectively. The rapid initial decay superimposed on the electron-spin relaxation is due to the hh-spin relaxation as explained above. The electron-spin decay is almost not affected by the change in temperature for both samples, while the hh-spin decay time is apparently shortened with increasing temperature and becomes lower than the time resolution of 130–200 fs at 100 K. From these results, it is thought that electron Mn spin scattering mechanism is temperature independent below 100 K. The drastic decrease of the hh-spin relaxation time with increasing temperature is related to the valence-band structure and hh momentum scattering by thermally activated phonon. As described in the preceding paragraph, the hh spin and lh spin are purely $J_z = \pm 3/2$ and $\pm 1/2$ only at Γ point, while they have the mixed spin state going away from the Γ point through the hh- and lh-band mixing. This means that any event of momentum scattering of the hole leads to the change in the hole spin state, which is in marked contrast to the case of an electron in the conduction band, where any momentum scattering of the electron does not change its spin state since the electron spin of $\pm 1/2$ is an eigenstate even at other than the Γ point. So the decrease of the hh-spin-relaxation time with increasing temperature is associated with the hh momentum scattering with thermally activated phonon.

V. SUMMARY

We have investigated carrier spin dynamics in $CdTe/Cd_{1-x}Mn_xTe$ QW's by means of the femtosecond time-resolved pump-probe experiment and have measured the transient CD spectra when the hh exciton is resonantly excited by the circularly polarized pulse. The measurement of the transient CD spectra enables us to determine directly the electron-spin relaxation separately from the hh-spin relaxation. We have also investigated the carrier spin dynamics in order to clarify the role of the s-d or p-d exchange interaction in their spin dynamics. We found that electron-spin-relaxation time is dramatically shortened with decreasing well width. We revealed the direct correlation between the spin-relaxation rate of the electron and its penetration degree into the magnetic barrier. This suggests that the Mn-spin should be a strong spin-flip scatter for the electron. The hh-spin relaxation was found to be insensitive to the well width compared to the electron-spin relaxation. This can be qualitatively understood by the trade-off relation between the hh-lh splitting and the penetration degree of hh into the magnetic barrier when the well width is changed.

Finally, we comment on the carrier spin-relaxation time in a magnetic field to proceed further study of the role of the s-d or p-d exchange interaction. On application of a magnetic field, the carrier spin-relaxation time generally has two contributions, the transverse spin relaxation time (T_2) and the longitudinal spin relaxation time (T_1) with respect to the direction of the magnetic field. The observable spin relaxation time (T_2^*) in the experiment can be expressed by $1/T_2^* \cong 1/T_2 + 1/2T_1$. So the present spin relaxation time that we observed in a zero field corresponds to $T_2^* \cong T_2$ since the Zeeman splitting of the degenerate spin levels is zero and we do not have to consider the longitudinal spin relaxation, that is, the energy relaxation. It would be difficult to extract only a field dependence of T_2 separated from T_1 in observable T_2^* in the experiment. The information of the role of the s-d or p-d exchange interaction is thought to be included in T_2 rather than T_1 since T_1 would become shorter for any samples under stronger magnetic field and resultant larger Zeeman splitting.

[1] A. Tackeuchi, S. Muto, T. Inata, and T. Fujii, Appl. Phys. Lett. **56**, 2213 (1990).
[2] S. Bar-Ad and I. Bar-Joseph, Phys. Rev. Lett. **68**, 349 (1992).
[3] T. Kawazoe, Y. Masumoto, and T. Mishina, Phys. Rev. B **47**, 10 452 (1993).
[4] Y. Takagi, S. Adachi, S. Takeyama, A. Tackeuchi, S. Muto, and J. J. Dubowski, J. Lumin. **58**, 202 (1994).
[5] Ph. Roussignol, P. Rolland, R. Ferreira, C. Delalande, G. Bastard, A. Vinattieri, L. Carraresi, M. Colocci, and B. Etienne, Surf. Sci. **267**, 360 (1992).
[6] A. Vinattieri, Jagdeep Shah, T. C. Damen, D. S. Kim, L. N. Pfeiffer, and L. J. Sham, Solid State Commun. **88**, 189 (1993).
[7] M. R. Freeman, D. D. Awschalom, J. M. Hong, and L. L. Chang, Phys. Rev. Lett. **64**, 2430 (1990).
[8] M. Kohl, M. R. Freeman, D. D. Awschalom, and J. M. Hong, Phys. Rev. B **44**, 5923 (1991).
[9] T. C. Damen, Luis Vina, J. E. Cunningham, Jagdeep Shah, and L. J. Sham, Phys. Rev. Lett. **67**, 3432 (1991).
[10] T. Kawazoe, T. Mishina, and Y. Masumoto, Jpn. J. Appl. Phys., Part 2 **32**, L1756 (1993).
[11] Y. Nishikawa, A. Tackeuchi, S. Nakamura, S. Muto, and N. Yohoyama, Appl. Phys. Lett. **66**, 839 (1995).
[12] H. Krenn, K. Kaltenegger, and G. Bauer, Solid-State Electron. **31**, 481 (1988).
[13] D. D. Awschalom and M. R. Freeman, Physica B **169**, 285 (1991).
[14] J. B. Stark, W. H. Knox, and D. S. Chemla, Phys. Rev. Lett. **68**, 3080 (1992).
[15] *Diluted Magnetic Semiconductors*, edited by J. K. Furdyna and J. Kossut (Academic, Tokyo, 1988), Vol. 25.
[16] S. Schmitt-Rink, D. S. Chemla, and D. A. B. Miller, Phys. Rev. B **32**, 6601 (1985).
[17] G. Bastard and L. L. Chang, Phys. Rev. B **41**, 7899 (1990).
[18] R. Ferreira and G. Bastard, Phys. Rev. B **43**, 9687 (1991).
[19] J. J. Baumberg, S. A. Crooker, D. D. Awschalom, N. Samarth, H. Luo, and J. K. Furdyna, Phys. Rev. B **50**, 7689 (1994).
[20] I. Brener, W. H. Knox, K. W. Goossen, and J. E. Cunningham, Phys. Rev. Lett. **70**, 319 (1993).
[21] A. Tackeuchi, Y. Nishikawa, and O. Wada, Appl. Phys. Lett. **68**, 797 (1996).
[22] Chris G. Van de Walle, Phys. Rev. B **39**, 1871 (1989).
[23] In the Kronig-Penney model calculation, the valence-band offset is determined to be 0.3 from the well width dependence of the energy splitting between the lowest heavy- and light-hole–exciton transitions ($e1$-hh1 and $e1$-lh1) and the well width dependence of energy on higher heavy-hole–exciton transitions ($e2$-hh2 and $e3$-hh3).
[24] S. A. Crooker, J. J. Baumberg, F. Flack, N. Samarth, and D. D. Awschalom, Phys. Rev. Lett. **77**, 2814 (1996).